

# Impairment of the Ubiquitin-Proteasome Pathway Is a Downstream Endoplasmic Reticulum Stress Response Induced by Extracellular Human Islet Amyloid Polypeptide and Contributes to Pancreatic $\beta$ -Cell Apoptosis

Sílvia Casas,<sup>1,2</sup> Ramon Gomis,<sup>1</sup> Fiona M. Gribble,<sup>3</sup> Jordi Altirriba,<sup>1</sup> Sakari Knuutila,<sup>4</sup> and Anna Novials<sup>2</sup>

**OBJECTIVE**—Human islet amyloid polypeptide (hIAPP) aggregation plays a major role in the development of islet amyloidosis in type 2 diabetes. It is known that extracellular hIAPP oligomers are toxic to pancreatic  $\beta$ -cells and associated with apoptosis. We therefore investigated the molecular mechanism by which extracellular hIAPP mediates pancreatic  $\beta$ -cell apoptosis.

**RESEARCH DESIGN AND METHODS**—MIN6 cells and primary cultures of human pancreatic islets were treated with freshly dissolved hIAPP peptide. Morphology of the cultures was evaluated by electron microscopy. Gene expression was analyzed by microarray, RT-PCR, and immunoblot. Calcium levels were measured in fura-2-loaded cells. Apoptosis was quantified by cytometry.

**RESULTS**—Increased expression of several heat shock proteins and activation of the spliced form of *XBP-1*, a transcription factor for overexpression of chaperones during endoplasmic reticulum (ER) stress, were detected together with morphological evidence of ER dysfunction. Intracellular calcium overload was detected in association with this process. Moreover, reduction in the proteasome activity, which was detected over time, contributed to the intracellular accumulation of ubiquitinated proteins, leading to a functional suppression of the ubiquitin-

proteasome pathway. In addition, impairment of the proteasome function contributed to apoptosis, while, despite the presence of hIAPP, cell viability improved when a proteasome activator was overexpressed. The key cytotoxic events induced by extracellular hIAPP were also observed in treated human islets.

**CONCLUSIONS**—Our data suggest that ER stress responses are intracellular signaling mechanisms induced by extracellular hIAPP aggregation and that impairment of the ubiquitin-proteasome pathway is implicated in ER stress-mediated pancreatic  $\beta$ -cell apoptosis. *Diabetes* 56:2284–2294, 2007

The presence of amyloid deposits within the pancreatic islets is a pathophysiological hallmark of type 2 diabetes (1,2). Islet amyloid polypeptide (IAPP), also known as amylin, is the main component of islet amyloid (3,4). It is produced by  $\beta$ -cells and cosecreted with insulin in response to nutrient stimuli (5–7). A target region between positions 20 and 29 is thought to be responsible for amyloid fibril formation by the human peptide (8). Several point mutations located in the human IAPP (hIAPP) promoter and missense point mutations on the encoding gene region have been identified by our group and others with different prevalence according to ethnic origin (9,10). However, because the sequence of hIAPP is identical in diabetic and nondiabetic individuals, the process of amyloid formation remains poorly understood.

Islet amyloid colocalizes with areas of cell degeneration, and the process of amyloidosis has been associated with progressive loss of pancreatic  $\beta$ -cell mass by apoptosis and, thus, much of the pathology of type 2 diabetes (11–14). A number of studies showed that the toxicity of hIAPP and other amyloidogenic peptides lies in the oligomeric intermediates rather than in the mature fibrils (15–17).

The endoplasmic reticulum (ER) integrates protein synthesis and folding and calcium storage and signaling. Several cellular stress conditions can cause ER dysfunction and protein misfolding (18). To overcome ER stress, cells initiate protective mechanisms, which are known as ER stress responses. One of these includes upregulation of heat shock proteins (HSPs), molecular chaperones responsible for recognizing the presence of misfolded proteins (19,20). Moreover, proteins that cannot be refolded

From the <sup>1</sup>Endocrinology and Diabetes Unit, Laboratory of Experimental Diabetes, IDIBAPS (Institut d'Investigacions Biomèdiques August Pi i Sunyer), Hospital Clinic and University of Barcelona, Barcelona, Spain; the <sup>2</sup>Institute of Diabetes, Sardà Farriol Foundation, Barcelona, Spain; the <sup>3</sup>Cambridge Institute for Medical Research, University of Cambridge, Department of Clinical Biochemistry, Wellcome Trust/MRC Building, Addenbrooke's Hospital, Cambridge, U.K.; and the <sup>4</sup>Laboratory of Cytomolecular Genetics, Department of Pathology, Haartman Institute, University of Helsinki and HUSLAB, Helsinki, Finland.

Address correspondence and reprint requests to Dr. Anna Novials, Institute of Diabetes, Sardà Farriol Foundation, Pg. Bonanova, 69, 6th floor, 08017 Barcelona, Spain. E-mail: anovials@fsf.es.

Received for publication 8 February 2007 and accepted in revised form 25 May 2007.

Published ahead of print at <http://diabetes.diabetesjournals.org> on 11 June 2007. DOI: 10.2337/db07-0178.

Additional information for this article can be found in an online appendix at <http://dx.doi.org/10.2337/db07-0178>.

ALLN, *N*-acetyl-Leu-Leu-norleucinal; EGFP, green fluorescent protein; ER, endoplasmic reticulum; FACS, fluorescence-activated cell sorting; FBS, fetal bovine serum; FITC, fluorescein isothiocyanate; hIAPP, human islet amyloid polypeptide; HSP, heat shock protein; IAPP, islet amyloid polypeptide; MODC, mouse ornithine decarboxylase; PI, propidium iodide; ROS, reactive oxygen species; RQ-PCR, real-time quantitative RT-PCR.

© 2007 by the American Diabetes Association.

The costs of publication of this article were defrayed in part by the payment of page charges. This article must therefore be hereby marked "advertisement" in accordance with 18 U.S.C. Section 1734 solely to indicate this fact.

must be eliminated. In the cytoplasm, the ubiquitin-proteasome proteolytic pathway is responsible for the clearance of intracellular misfolded and aggregated proteins (20,21). However, when severe and prolonged ER stress extensively impairs ER functions, the ultimate response is apoptosis (18). Pancreatic  $\beta$ -cells are sensitive to ER stress, and ER stress-mediated apoptosis has been associated with  $\beta$ -cell loss (22).

A common mechanism for initiation of cytotoxicity, which has been observed for all the amyloid oligomers studied to date, is their capacity to elevate intracellular calcium and reactive oxygen species (ROS), mediated by plasma membrane perturbation when formed and deposited extracellularly (15–17,23–28). Both intracellular alterations can cause ER dysfunction (18). Interestingly, ER stress responses have been described in neurons exposed to extracellular amyloidosis (29–31). Consistent with these observations, we hypothesized that ER stress responses could be associated with extracellular hIAPP aggregates, with consequent induction of pancreatic  $\beta$ -cell dysfunction. The aim of the present study was to investigate the molecular mechanisms by which extracellular hIAPP promotes pancreatic  $\beta$ -cell apoptosis.

## RESEARCH DESIGN AND METHODS

**Cell culture.** MIN6 cells (32) were cultured in Dulbecco's modified Eagle's medium media containing 5.5 mmol/l glucose and supplemented with 10% fetal bovine serum (FBS), 2 mmol/l L-glutamine, 5  $\mu$ mol/l  $\beta$ -mercaptoethanol, 100 units/ml penicillin, and 100  $\mu$ g/ml streptomycin at 37°C with 5% CO<sub>2</sub>.

**Human pancreatic islet isolation and culture.** Pancreases were obtained from 11 human cadaveric organ donors (4 men and 7 women, 41  $\pm$  17 years of age, BMI 23  $\pm$  5 kg/m<sup>2</sup>), after informed consent of their families and approval of the hospital ethics committee. Islets were isolated by collagenase digestion of the pancreas (SERVA Electrophoresis, Heidelberg, Germany) and separated from exocrine tissue by Biocoll density gradient (Biochrom, Berlin, Germany), as previously described (6). Islets were transferred to RPMI-1640 medium (Gibco-BRL, Paisley, U.K.) containing 11.1 mmol/l glucose and supplemented with 10% FBS, 2 mmol/l L-glutamine, 100 units/ml penicillin, and 100  $\mu$ g/ml streptomycin and cultured overnight at 37°C with 5% CO<sub>2</sub>. Islets were then picked and cultured in 5.5 mmol/l glucose.

**Chemicals.** Synthetic human and rat IAPP (Bachem, Bubendorf, Switzerland) were dissolved in sterile water at 500  $\mu$ mol/l and incubated at room temperature for 10 min before use at 1, 10, or 20  $\mu$ mol/l in culture. Epoxomicin and N-acetyl-Leu-Leu-norleucinal (ALLN) (Calbiochem, Darmstadt, Germany) were dissolved in ethanol at 1.5 and 5.2 mmol/l stock solution before use at 10 and 30  $\mu$ mol/l, respectively, in culture.

**Transmission electron microscopy.** For ultrastructural analysis of the insoluble aggregates, a 4- $\mu$ l sample of suspension was applied onto a formvar carbon-coated copper grid for 1 min, dried, stained with 2% (wt/vol) uranyl acetate in water for 1 min, and air-dried. For cellular ultrastructural analysis, MIN6 cells of the same culture were fixed in glutaraldehyde 2.5% (wt/vol) in 0.1 mol/l phosphate buffer at 4°C for 1.5 h, rinsed in 0.1 mol/l phosphate buffer, and postfixed in osmium tetroxide 1% (wt/vol) in the same buffer for 1 h. The samples were dehydrated, embedded in Spurr, and polymerized at 60°C for 48 h. Ultrathin sections (60–90 nm) were cut, placed on 200 mesh copper grids, and doubled stained with 2% (wt/vol) uranyl acetate and lead citrate. Grids were examined using a Jeol 1010 transmission electron microscope (Jeol, Tokyo, Japan) operating at 80 kV.

**Apoptosis assays.** Cells were stained with annexin V-fluorescein isothiocyanate (FITC) and propidium iodide (PI) using Annexin V-FITC Apoptosis Detection Kit (Becton Dickinson, San Jose, CA). Thereafter, cells were analyzed by fluorescence-activated cell sorting (FACS) within 1 h on a FACS Calibur with Cell Quest software (Becton Dickinson). Annexin V-FITC- and PI-negative cells are viable cells. Early apoptotic cells are annexin V-FITC positive. Cells both positive for annexin V-FITC and PI are dead cells, either as a result of late apoptosis or necrosis. Movement of cells through these three stages indicates apoptosis and not necrosis.

**Islet cell viability analysis.** The protocol for isolation of single islet cells was as published previously (33). Human islets were digested in PBS containing 0.125 mg/ml trypsin and 0.05 mg/ml EDTA at 37°C. The cell suspension was cycled for 5 min on ice to allow islets to sediment. The supernatant containing single cells was removed and placed in FBS. To obtain

additional single islet cells, the digestion process was repeated three times. Cells were washed with PBS and stained with PI (Becton Dickinson). FACS was performed within 1 h on FACS Calibur with Cell Quest software (Becton Dickinson). PI-negative cells were counted as viable cells.

**Calcium measurements.** Cells were grown on 35-mm glass-bottom culture dishes (MatTek, Ashland, MA). Medium was replaced with assay buffer, namely Krebs-Ringer bicarbonate solution at 1 mmol/l glucose. Cells were then loaded with fura-2 acetoxyethyl ester (Molecular Probes, Leiden, Netherlands) at 5  $\mu$ mol/l for 30 min. A digital epifluorescence imaging system (Cairn Research, Faversham, U.K.) mounted on an inverted fluorescence microscope (Olympus IX71, Southall, U.K.) was used to measure calcium levels. Ratiometric images of excitation at 340 and 380 nm were collected using Universal Imaging MetaFluor software (Cairn Research) and recorded with a charged-coupled device camera (Hammamatsu Orca ER; Cairn Research). Minimal and maximal signals were determined with 5  $\mu$ mol/l ionomycin in 5 mmol/l EGTA/0 mmol/l Ca<sup>2+</sup> and 5 mmol/l Ca<sup>2+</sup>, respectively, at the end of the experiment.

### Gene expression analyses

**RNA isolation.** Total RNA was extracted using the RNeasy Mini Kit (Qiagen, Hilden, Germany) performing on-column DNase digestion with RNase-Free DNase Set (Qiagen). The RNA quality was checked on a Bioanalyzer 2100 (Agilent Technologies, Palo Alto, CA).

**Microarray analysis.** Ten micrograms of pooled total RNA derived from three independent experiments was converted into cRNA, and thereafter 20  $\mu$ g of biotin-labeled cRNA was fragmented to a mean size of 35–200 bases and then hybridized to Mouse GeneChip 430A array (Affymetrix, Santa Clara, CA). Following hybridization, microarrays were washed and stained with streptavidin-R-phycoerythrin (Molecular Probes, Eugene, OR) using GeneChip Fluidics Station 400 (Affymetrix). After scanning, images were converted to files by Affymetrix Microarray Suite software. The data were deposited in NCBI's Gene Expression Omnibus (GEO, <http://www.ncbi.nlm.nih.gov/geo/>) and are accessible through GEO Series accession number GSE2253. Detailed description of microarray quality controls and data analysis can be found in the online appendix of the supplementary methods (available at <http://dx.doi.org/10.2337/db07-0178>).

**Real-time quantitative RT-PCR.** cDNA was synthesized from 0.5  $\mu$ g total RNA using a cDNA Synthesis Kit (Roche Diagnostics, Mannheim, Germany). The oligonucleotide primers were: 5'-CGGACGCTCTGGATAAAAATCC-3' and 5'-TCCTTCCCAGTCAGTTT-3' for mouse HSP 90 kDa  $\alpha$  (cytosolic) class A member 1 (*Hsp90aa1*), 5'-CCTGGGAACCATGCTAAGTCT-3' and 5'-GCCCCATCATGGAGATGTCT-3' for mouse Hsp90  $\alpha$  class B member 1 (*Hsp90ab1*), 5'-CACACTAGGTCGTGGAACAACA-3' and 5'-TCTGTCTTGCTA CTCACACGT-3' for mouse Hsp90  $\beta$  member 1 (*Hsp90b1*), 5'-GTGGAGGA GTTCAAGAGAAAACAACA-3' and 5'-TCACGGCTCGCTTGTCTG-3' for human *HSP90AA1*, 5'-TGGCAGTCAAGCACTTTTCTGT-3' and 5'-GCCCGACGA GGAATAAATAGC-3' for human *HSP90AB1*, and 5'-TGTTTCCCAGACTC TTC-3' and 5'-TGTCAGCTGTTTACGAACAAG-3' for human *HSP90B1*. Real-time quantitative RT-PCR (RQ-PCR) was performed with 0.5 ng cDNA using SYBR Green Reagents and the ABI Prism 7900HT Sequence Detection System (Applied Biosystems, Foster City, CA). A standard curve of each primer set was generated from serial dilutions of cDNA. The PCR products were verified using dissociation curve analysis using SDS software (Applied Biosystems). 18S rRNA (Applied Biosystems) was used to normalize expression.

**RT-PCR analysis of Xbp-1 splicing.** Fifty nanograms of cDNA was used for PCR with 5'-GAACCAGGAGTTAAGAACACG-3' and 5'-AGGCAACAGTGTCA-GAGTCC-3' primers from mouse X-box binding factor-1 (*Xbp-1*) mRNA. PCR products were separated by electrophoresis on a 2.5% agarose gel and visualized by ethidium bromide staining. Unspliced and spliced *Xbp-1* gave products of 205 and 179 bp, respectively. The percentage of s*Xbp-1* to total *Xbp1* was determined by densitometry using Quantity One software (Bio-Rad Laboratories, Hercules, CA).

**Immunoblot analyses.** Cell lysate protein aliquots of 10–30  $\mu$ g were separated by SDS-PAGE on 8–15% polyacrylamide gels and transferred to polyvinylidene fluoride. Primary antibodies used were anti-active caspase-3 (Abcam, Cambridge, U.K.), anti-HSP90B1 (ABR Affinity Bioreagents, Golden, CO), anti- $\beta$ -actin (Sigma-Aldrich, Saint Louis, MO), anti-HSP90AA1, and anti-HSP90AB1 (both from Kamiya Biomedical, Seattle, WA). Changes in protein levels were evaluated by Quantity One software (Bio-Rad Laboratories).

### Proteasome activity assays

**Quantification of proteasome activity in living cells.** In the pZsProSensor-1 reporter (Clontech, Palo Alto, CA), fluorescent green protein (ZsGreen) is fused to the mouse ornithine decarboxylase (MODC) degradation domain. Since the MODC degradation domain targets the constitutively expressed protein for rapid degradation, the protein does not accumulate in cells until the proteasome is inhibited. The pUb<sup>G76V</sup>-EGFP reporter (kindly provided by Dr. Dantuma, Karolinska Institutet, Sweden) carries an ubiquitin fusion degradation-targeted enhanced green fluorescent protein (EGFP) (34). Either



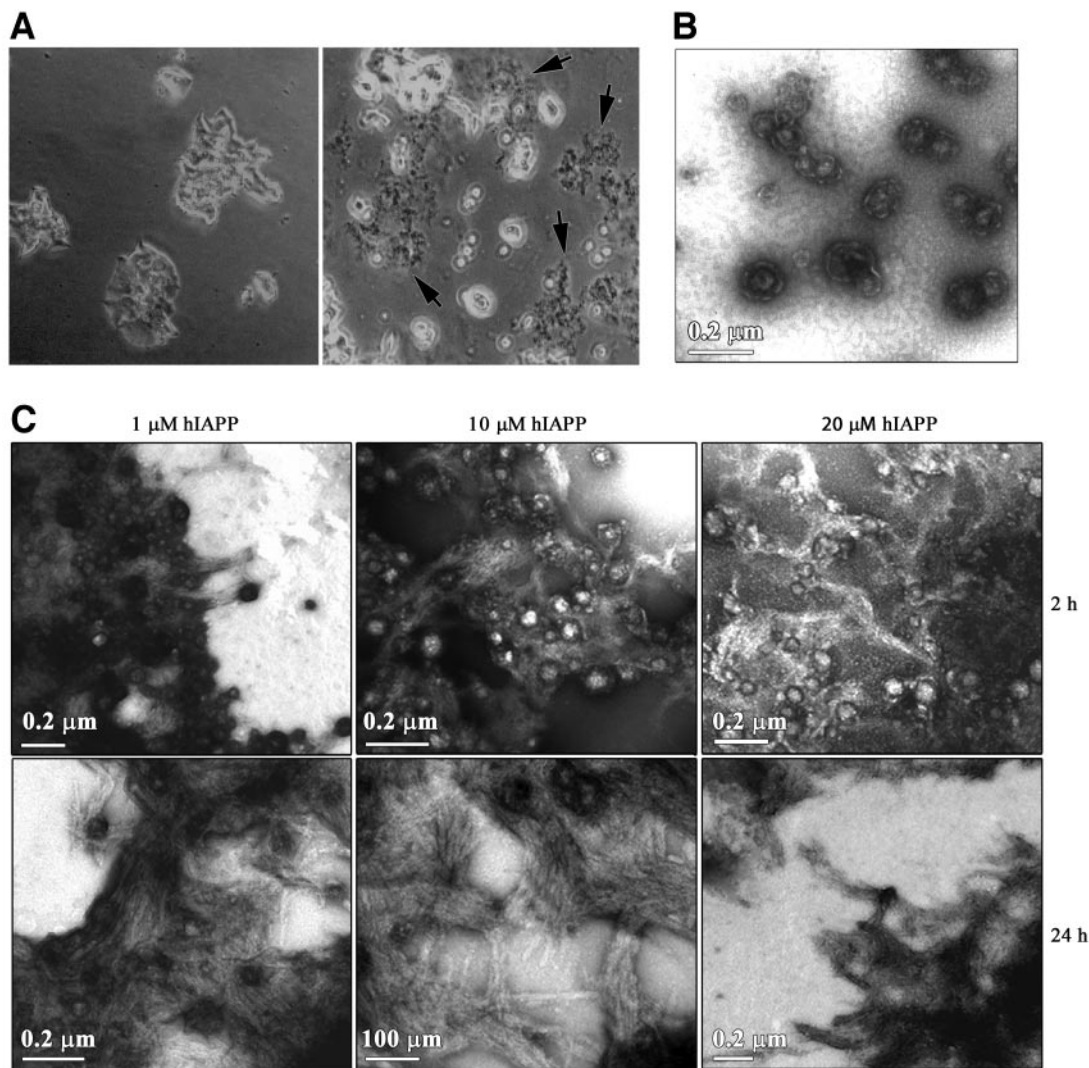


**FIG. 1.** Analysis of hIAPP aggregation. **A:** Insoluble aggregates (arrowhead) were observed in culture medium of MIN6 cells after 45 min with 1, 10, and 20 μmol/l hIAPP compared with the control. Original magnification  $\times 40$ . **B:** Morphology of hIAPP aggregates was assessed by electron microscopy. Prefibrillar hIAPP structures were first observed after 10 min of treatments. **C:** At 2 h, hIAPP fibrils were detected being formed from prefibrillar hIAPP structures (upper panels). At 24 h, prefibrillar hIAPP structures were still observed, although most of them had already been transformed to fibril form (lower panels). Original magnifications are indicated.

pZsProSensor-1 or pUb<sup>G76V</sup>-EGFP was transfected into MIN6 cells using Lipofectamine 2000 (Invitrogen, Carlsbad, CA). After overnight incubation, treatments were initiated and fluorescence monitored using FACS Calibur with Cell Quest software (Becton Dickinson).

**Human 20S proteasome activity assay.** Aliquots of 50 μg protein from human pancreatic islet lysate were tested for proteasome activity using 20S proteasome activity assay kit (Chemicon International, Temecula, CA). Detections were made by spectrofluorometry (SpectraMax GeminiXS; Molecular Devices, Sunnyvale, CA), setting excitation and emission wavelengths at 380 and 460 nm, respectively.

**Delivery of proteasome activator.** Ten micrograms of protein activator 28 (PA28; Calbiochem) or vehicle control were transfected into MIN6 cells using Lipofectamine 2000 (Invitrogen). After 4 h of incubation, the culture medium was changed and cells treated with or without 10 μmol/l hIAPP for 16 h. For the apoptosis positive control, MIN6 cells were irradiated 4 h after transfection with 50 Gy using a source of <sup>137</sup>Cs (Gamma Cell 1000; Atomic Energy of Canada Limited Commercial Products, Ottawa, Canada) and returned to culture for an additional 16 h.

**RESULTS**

**Analysis of hIAPP aggregation.** MIN6 cells were cultured with 1, 10, or 20 μmol/l freshly dissolved hIAPP peptide for 2, 12, or 24 h. Insoluble aggregates were observed under an inverted microscope at  $\times 40$  magnifica-

tion in the culture media of all experiments from 45 min of treatment onwards (Fig. 1A). The process of hIAPP aggregation was evaluated over time by examining the peptide conformational state of hIAPP in the culture media by electron microscopy. At 10 min after treatment, hIAPP peptide precipitated in a prefibrillar form, consisting of spherical vesicles of 5–10 nm in diameter, assembled in spheroids of 80–100 nm in diameter (Fig. 1B). The ultrastructural morphology of hIAPP aggregates resembled that reported for β-amyloid peptide oligomers (16), and the observation of prefibrillar spheroids has been published previously (25). The maximum formation of these hIAPP prefibrillar structures was achieved at 45 min. hIAPP fibrils were first detected at 2 h, being formed among the hIAPP oligomeric forms (Fig. 1C). At 24 h, hIAPP prefibrillar structures were still observed, although most of the hIAPP peptide had acquired a fibrillar conformation (Fig. 1C).

**Effects of extracellular hIAPP on MIN6 cells.** Significant decreases in MIN6 cell viability were detected in the culture conditions where hIAPP aggregates were being formed (Fig. 2A). A decline in viability of the MIN6 cells

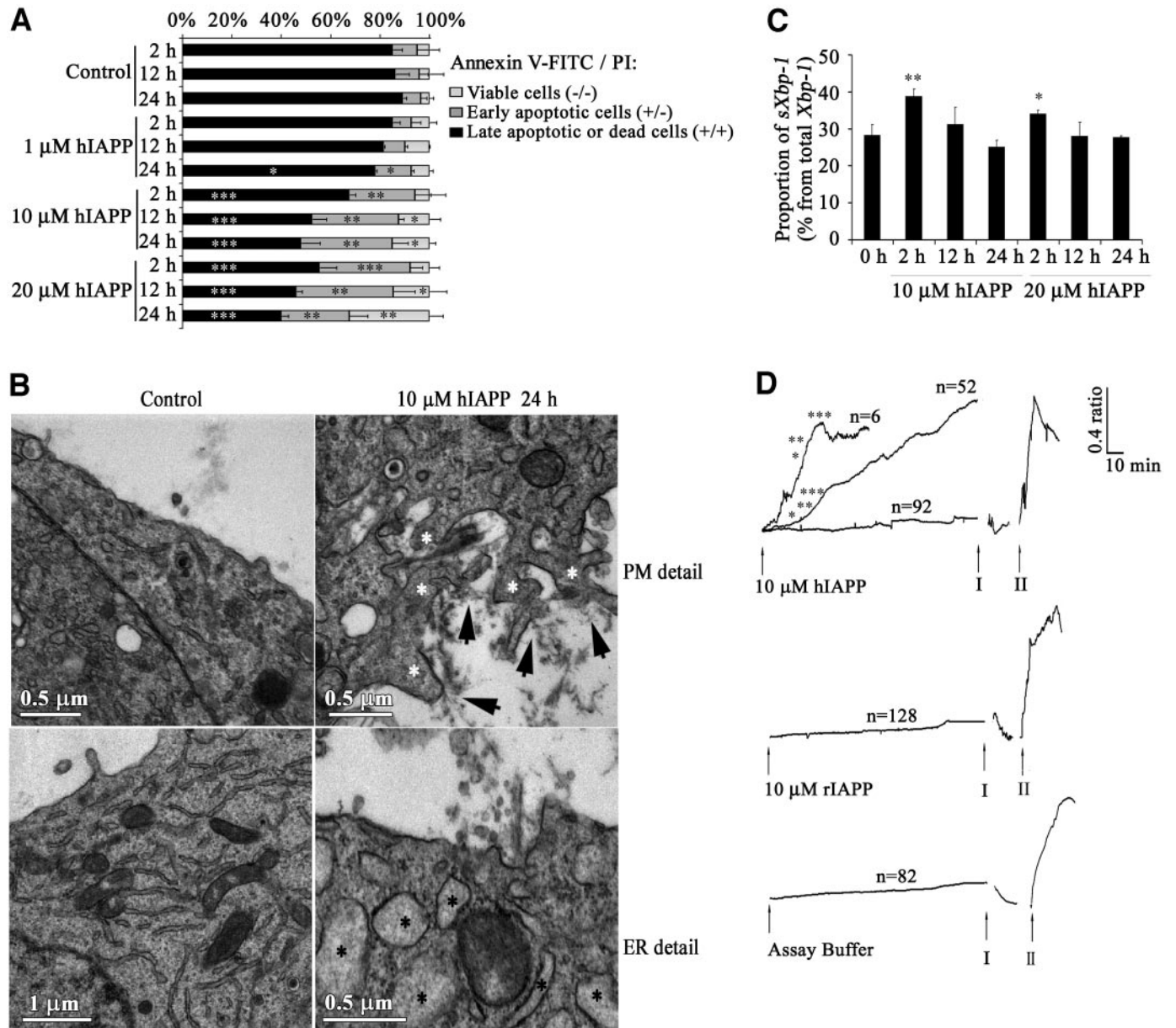


**FIG. 2.** Effect of extracellular hIAPP on MIN6 cells. **A:** Apoptosis assay on MIN6 cells treated with 1, 10, or 20  $\mu\text{mol/l}$  hIAPP compared with the control. Cell staining with annexin V-FITC and PI was analyzed by FACS. Results are means  $\pm$  SD ( $n = 6$ ) ( $*P < 0.05$ ,  $**P < 0.01$ ,  $***P < 0.001$ ; by ANOVA). **B:** Morphological analysis of MIN6 cells exposed to extracellular hIAPP compared with the control. *Upper panels* show how hIAPP aggregates were located close to the cell margins (arrows). The plasma membrane (PM) was irregular and showed prominent invaginations (asterisks). *Lower panels* show abnormal morphology of ER (asterisks) in treated MIN6 cells. All panels correspond to MIN6 cells cultured for 24 h with 10  $\mu\text{mol/l}$  hIAPP compared with the control. Original magnifications are indicated. **C:** RT-PCR analysis of *Xbp-1* splicing was performed with primers flanking the intron excised from mouse *Xbp-1* mRNA. The percentage of *sXbp-1* to total *Xbp-1* determined by densitometry is illustrated. Results are means  $\pm$  SD ( $n = 4$ ) ( $*P < 0.05$ ,  $**P < 0.01$ ; by Mann-Whitney test). **D:** Intracellular calcium concentration was monitored for 2 h as the 340/380-nm fluorescence ratio in fura-2-loaded MIN6 cells after treatment with either 10  $\mu\text{mol/l}$  hIAPP (*upper plot*) or rIAPP (*middle plot*). Baseline ratio of MIN6 cells was recorded in assay buffer (*lower plot*). Results are mean 340/380-nm fluorescence ratio over time of the total number of recorded MIN6 cells in at least three independent experiments. Significant changes in the mean 340/380-nm fluorescence ratio were detected with 10  $\mu\text{mol/l}$  hIAPP compared with the baseline ratio ( $*P < 0.05$ ,  $**P < 0.01$ ,  $***P < 0.001$ ; by ANOVA). Minimal and maximal signals were recorded in the presence of 5  $\mu\text{mol/l}$  ionomycin in 5 mmol/l EGTA/0 mmol/l Ca<sup>2+</sup> (I) and 5 mmol/l Ca<sup>2+</sup> (II), respectively, at the end of the experiments.

was already detected at 2 h with 10 and 20  $\mu\text{mol/l}$  hIAPP compared with the control. At these concentrations, there were primarily two populations: cells that were viable and cells initiating apoptosis. Follow-up at 12 and 24 h revealed a decrease in viable cells and an augmentation of early apoptotic cells. The proportion of late apoptotic cells increased significantly at 24 h with 20  $\mu\text{mol/l}$  hIAPP. Significant increases in the proportion of early apoptotic

cells were observed at 24 h with 1  $\mu\text{mol/l}$  hIAPP compared with the control.

The morphology of MIN6 cells was studied by electron microscopy in the respective experimental conditions. Images revealed that extracellular hIAPP insoluble forms interacted with the plasma membrane (Fig. 2B). In these regions, the plasma membrane was irregular and presented deep invaginations compared with the control.

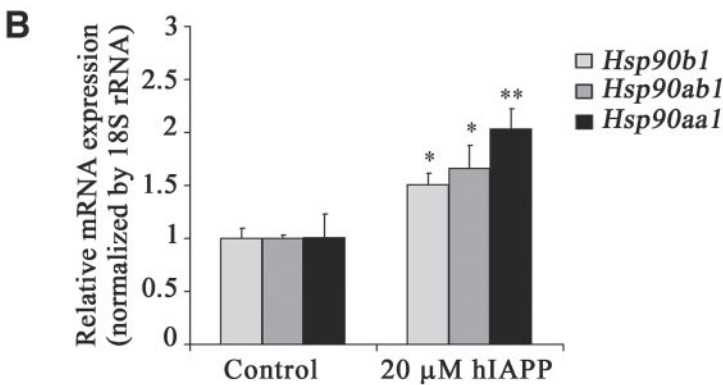
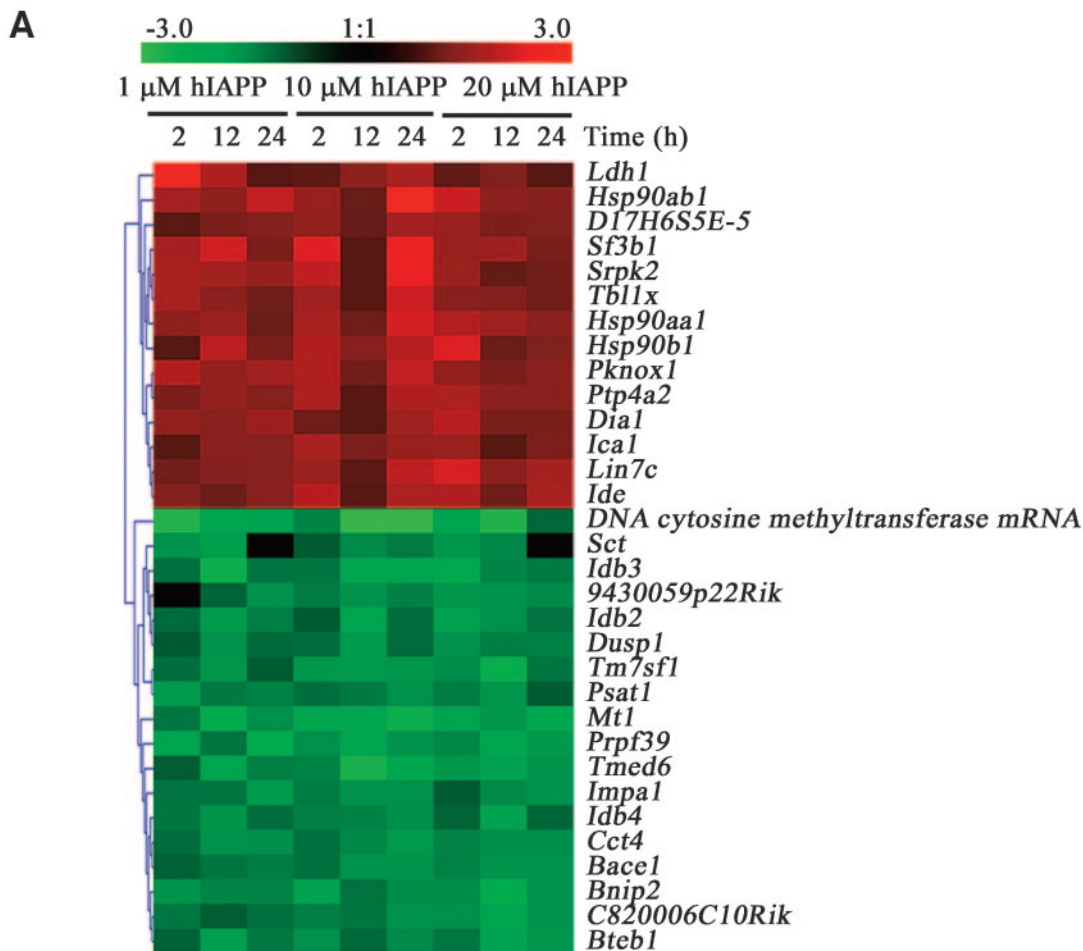


**FIG. 3.** Identification of gene expression changes induced by extracellular hIAPP. **A:** Microarray analysis detected 32 deregulated genes with expression values that were significantly altered by hIAPP treatment according to a fold change of 1.5 in at least three of the nine follow-up experimental conditions. Hierarchical clustering analysis on the basis of gene expression is shown. The color intensity correlates with the expression fold change compared with control, ranging from -3 to 3. Gene name is indicated on the right, while experimental condition is on the top. **B:** Overexpression of *Hsp90aa1*, *Hsp90ab1*, and *Hsp90b1* by extracellular hIAPP treatment was confirmed by RQ-PCR in MIN6 cells treated with 20 μmol/l hIAPP for 24 h compared with the control. Results are means ± SD ( $n = 6$ ) (\* $P < 0.05$ , \*\* $P < 0.01$ ; by Mann-Whitney test).

Moreover, treated MIN6 cells exhibited modified ER morphology, characterized by accumulation of protein aggregates within the ER lumen and increased ER size (Fig. 2B). Activation of the ER stress response was assessed by measuring the activation of Xbp-1. Exposure to 10 and 20 μmol/l hIAPP for 2 h significantly increased splicing of *Xbp-1* (Fig. 2C). From 12 h after treatment, the increase of the *sXbp-1* product had returned to basal levels (Fig. 2C).

We next examined whether the observed phenotype was associated with changes in intracellular calcium levels. Measurements of the 340/380-nm fluorescence ratio were monitored for 2 h in fura-2-loaded MIN6 cells without treatment ( $n = 87$ ) to obtain the mean baseline ratio (Fig. 2D). MIN6 cells treated with 10 μmol/l hIAPP were divided into three subpopulations based on their response profiles (Fig. 2D). Thirty-five percent of cells (52 of 150) exhibited

a continuous increase in the 340/380 ratio, statistically significant from 16 min after treatment onward, compared with the mean baseline ratio. Four percent of cells (6 of 150) exhibited a rapid and acute increase in the mean 340/380 ratio, significant from 30 min after treatment onward. In both subpopulations, calcium responses went high and failed to recover. Cells lost their adherent properties after achieving the maximum responses, at which time subsequent fluorescence measurements were also lost. The remaining 61% of cells were counted as nonresponsive (92 of 150). No appreciable increase in the mean 340/380 ratio was observed with 10 μmol/l hIAPP (Fig. 2D). **Gene expression changes induced by extracellular hIAPP.** Microarray technology was applied to study changes in global gene expression under the different experimental conditions over time. Analysis of microarray



TABLE 1  
Genes detected by microarray data analysis

Biological process	Gene name	Gene accession no.	Expression
Heat shock proteins	HSP 90 kDa $\alpha$ (cytosolic) class A member 1 ( <i>Hsp90aa1</i> )	Mm0.1843	Up
	HSP 90 kDa $\alpha$ (cytosolic) class B member 1 ( <i>Hsp90ab1</i> )	Mm0.2180	Up
	HSP 90 kDa $\beta$ member 1 ( <i>Hsp90b1</i> )	Mm0.87773	Up
Proliferation	Inhibitor of DNA binding 2 ( <i>Idb2</i> )	Mm0.34871	Down
	Inhibitor of DNA binding 3 ( <i>Idb3</i> )	Mm0.110	Down
	Inhibitor of DNA binding 4 ( <i>Idb4</i> )	Mm0.28223	Down
Apoptosis	Dual-specificity phosphatase 1 ( <i>Dusp1</i> )	Mm0.239041	Down
	BCL2/adenovirus E1B 19 kDa interacting protein 1, NIP2 ( <i>Bnip2</i> )	Mm0.159777	Down
Regulation of gene transcription	Transducin ( $\beta$ )-like 1 X-linked ( <i>Tbl1x</i> )	Mm0.258476	Up
	Pbx/knotted 1 homeobox ( <i>Pknox1</i> )	Mm0.259295	Up
	Basic transcription element binding protein 1 ( <i>Bteb1</i> )	Mm0.291595	Down
mRNA processing	Splicing factor 3b, subunit 1 ( <i>Sf3b1</i> )	Mm0.279736	Up
	PRP39 pre-mRNA processing factor 39 homolog (yeast) ( <i>Prpf39</i> )	Mm0.283339	Down
Protein amino acid des-phosphorylation	Serine/arginine-rich protein specific kinase 2 ( <i>Srpk2</i> )	Mm0.288728	Up
	Protein tyrosine phosphatase 4a2 ( <i>Ptp4a2</i> )	Mm0.193688	Up
Cell transmembrane component	Transmembrane emp24 protein transport domain containing 6 ( <i>Tmed6</i> )	Mm0.23032	Down
	Transmembrane 7 superfamily member 1 ( <i>Tm7sf1</i> )	Mm0.362142	Down
	Transmembrane protein 46 ( <i>9430059P22Rik</i> )	Mm0.275409	Down
ESTs	RIKEN cDNA C920006C10 gene ( <i>C920006C10Rik</i> )	Mm0.260647	Down
	DNA segment, Chr 17, human D6S56E 5 ( <i>D17H6S56E-5</i> )	Mm0.22506	Up
	Lin 7 homolog c ( <i>C. elegans</i> ) ( <i>Lin7c</i> )	Mm0.235300	Up
Cell-cell junctions	Lactate dehydrogenase 1, A chain ( <i>Ldh1</i> )	Mm0.29324	Up
Cell metabolism	Diaphorase 1 (NADH) ( <i>Dia1</i> )	Mm0.22560	Up
	Phosphoserine aminotransferase 1 ( <i>Psat1</i> )	Mm0.289936	Down
	Inositol (myo)-1(or 4)-monophosphatase 1 ( <i>Impa1</i> )	Mm0.183042	Down
	Secretin ( <i>Sct</i> )	Mm0.4723	Down
Hormone	Insulin degrading enzyme ( <i>Ide</i> )	Mm0.28366	Up
	Beta-site APP cleaving enzyme 1 ( <i>Bace1</i> )	Mm0.24044	Down
Protein degradation	Chaperonin subunit 4 (delta) ( <i>Cct4</i> )	Mm0.296985	Down
	Metallothionein 1 ( <i>Mt1</i> )	Mm0.192991	Down
Protein folding	Islet cell autoantigen 1 ( <i>Ica1</i> )	Mm0.275683	Up
Metal ion binding	DNA cytosine methyltransferase mRNA	AF071754	Down
Secretore trafficking			
DNA methylation			

data revealed 32 putative target genes whose expression was dose- and time-dependently altered by hIAPP treatment (Fig. 3A and Table 1). We focused on *Hsp90aa1*, *Hsp90ab1*, and *Hsp90b1*, whose expression was increased in hIAPP-treated cells compared with the control. To corroborate microarray data and to obtain quantitative gene expression values, transcript levels were quantified by RQ-PCR. Expression of *Hsp90aa1*, *Hsp90ab1*, and *Hsp90b1* in MIN6 cells increased significantly following treatment with 20  $\mu\text{mol/l}$  hIAPP for 24 h compared with the control (Fig. 3B).

#### Effect of extracellular hIAPP on proteasome activity.

To address whether proteasome function was affected by extracellular hIAPP aggregates, we transiently expressed ZsGreen-MODC fluorescent protein in MIN6 cells. Application of hIAPP evoked a rapid increase in the proportion of green fluorescence cells, which was significantly detected at 2 h in the presence of 10 and 20  $\mu\text{mol/l}$  hIAPP and at 24 h with 1  $\mu\text{mol/l}$  hIAPP (Fig. 4A). No changes in proteasome function were detected by administration of rIAPP (Fig. 4A). Suppression of proteasome activity can alternatively be detected by intracellular accumulation of ubiquitinated proteins. We verified the effects of extracellular hIAPP on the blocking of proteasome activity by measuring ubiquitinated proteins in MIN6 cells transiently transfected with Ub<sup>G76V</sup>-EGFP. Accumulation of the reporter was significantly detected in MIN6 cells from 2 h onwards with 20  $\mu\text{mol/l}$  hIAPP and at 24 h with 1 and 10

$\mu\text{mol/l}$  hIAPP (Fig. 4B). There was no deposition of the reporter with rIAPP treatment (Fig. 4B).

**Effect of proteasome activity on MIN6 cells.** To study the effects of impairment of the ubiquitin-proteasome pathway on pancreatic  $\beta$ -cells, loss-of-function experiments were performed using two different inhibitors of proteasome-dependent proteolysis. FACS analysis with annexin V-FITC and PI showed that treatment of MIN6-cells with either 10  $\mu\text{mol/l}$  epoxomicin or 30  $\mu\text{mol/l}$  ALLN significantly reduced cell viability from 24 h in culture onwards compared with the vehicle control (Fig. 5A). The effect of proteasome-dependent proteolysis inhibitors was associated with an increase in apoptosis (Fig. 5A).

Moreover, we tested whether enhancement of proteasome activity may improve viability of MIN6 cells exposed to extracellular hIAPP. Proteasome function was stimulated by the proteasome activator PA28, directly delivered into the cells by lipofection. After 16 h of culture with 10  $\mu\text{mol/l}$  hIAPP peptide, apoptotic signaling of MIN6 cells was associated with caspase cascade activation, detected by an increase in the active caspase-3 fraction (Fig. 5B and C). Likewise, when we stimulated the proteasome function with PA28, there was a significant recovery of cell viability and reduced caspase-3 activation despite the presence of 10  $\mu\text{mol/l}$  hIAPP (Fig. 5B and C). These data suggested that the inhibition of the ubiquitin-proteasome pathway was an upstream activator of apoptosis. PA28 had no effect on caspase-3 activation or cell viability by itself (Fig.

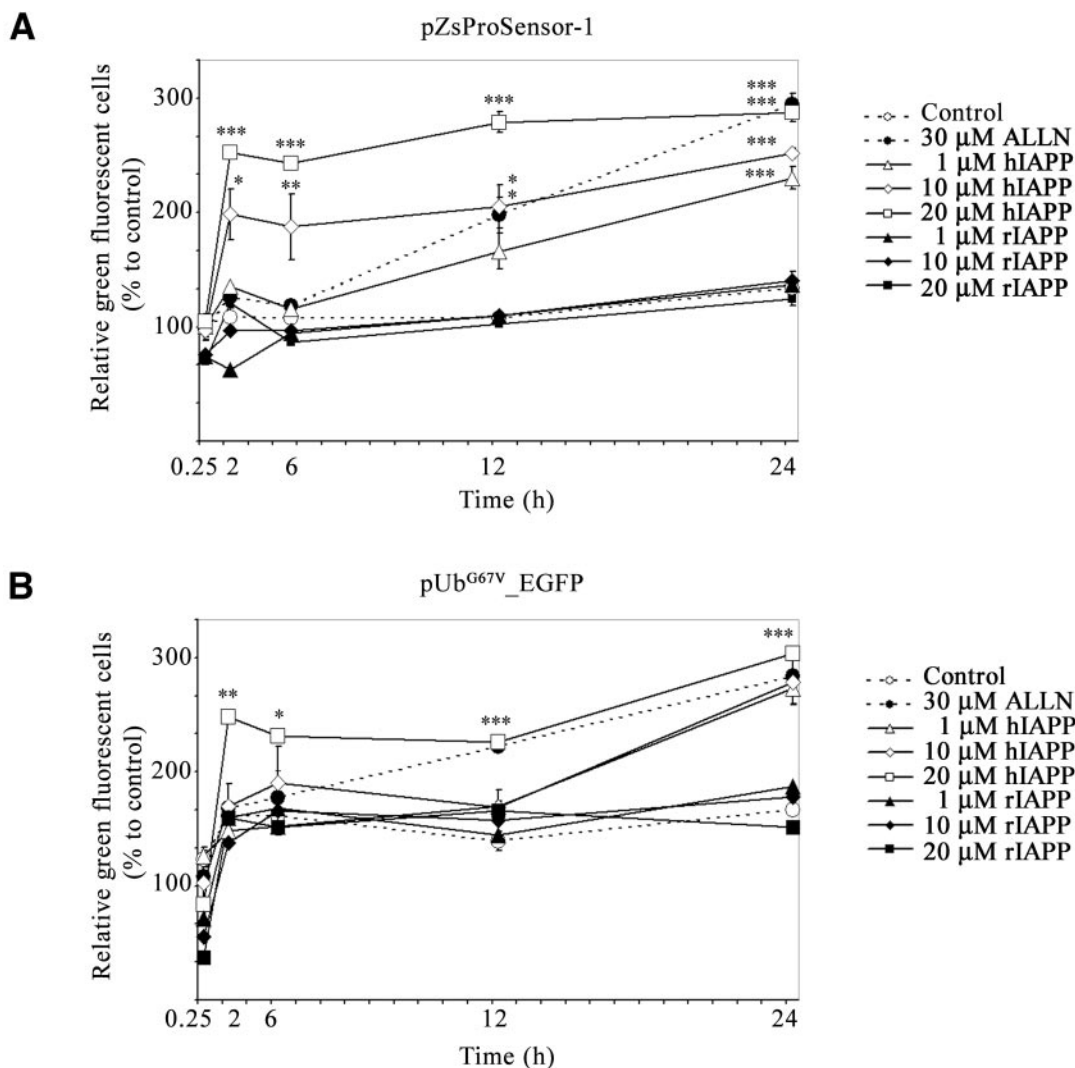


**FIG. 4.** Effect of extracellular hIAPP on proteasome activity. MIN6 cells were transiently transfected with pZsProSensor-1 (A) or pUb<sup>G67V</sup>-EGFP (B) reporter and treated with 1, 10, or 20 μmol/l hIAPP or rIAPP. As a positive control, cells were treated with 30 μmol/l ALLN. The negative control was cells exposed to ALLN vehicle solution. Positive green fluorescence cells were analyzed by FACS. Results are means ± SD (n = 6) (\*P < 0.05, \*\*P < 0.01, \*\*\*P < 0.001; by ANOVA).

5B and C). Furthermore, an apoptotic control induced by DNA damage was included, an insult that activates apoptosis independently of the proteasome pathway. After a gamma irradiation of 50 Gy, the active caspase-3 fraction increased along with apoptosis compared with the control, and it was not reversed by the addition of PA28 (Fig. 5B and C).

**Effect of extracellular hIAPP on human islets.** Based on the present findings, we next investigated in primary cultures of human pancreatic islets whether we could confirm the key observed effects of extracellular hIAPP cytotoxicity. After 24 h treatment with 10 and 20 μmol/l hIAPP, viability of human islet cell populations decreased significantly compared with the control (Fig. 6A). Expression of *HSP90AA1*, *HSP90AB1*, and *HSP90B1* was significantly upregulated in human pancreatic islets after 48 h of treatment with 20 μmol/l hIAPP (Fig. 6B), expression changes that were corroborated at the protein level (Fig. 6C). Treatment with either 10 μmol/l epoxomicin or 30 μmol/l ALLN for 48 h significantly reduced islet cell viability compared with the vehicle control (Fig. 6D). Furthermore, protein extracts from human pancreatic

islets incubated with 20 μmol/l hIAPP for 24 h showed decreased proteasome activity compared with the control when these were tested in a fluorometric 20S proteasome activity assay (Fig. 6E).

**DISCUSSION**

Pancreatic MIN6 β-cells were cultured at different times with different concentrations of freshly dissolved hIAPP to obtain spontaneous formation of hIAPP oligomers. In these cultures, markers of ER stress were detected. Among them, microarray analysis revealed increased expression of *HSP90AA1*, *HSP90AB1*, and *HSP90B1*. These gene expression changes were further confirmed in primary cultures of human pancreatic islets exposed to extracellular hIAPP. *HSP90B1* encodes a resident ER luminal stress protein, which together with cytosolic *HSP90AA1* and *HSP90B1* belongs to the *HSP90* family of molecular chaperones (35). Overexpression of HSPs is induced by the presence of misfolded proteins within the ER to rescue their conformation and prevent aggregation (18,19). XBP-1 is a key transcription factor for overexpres-

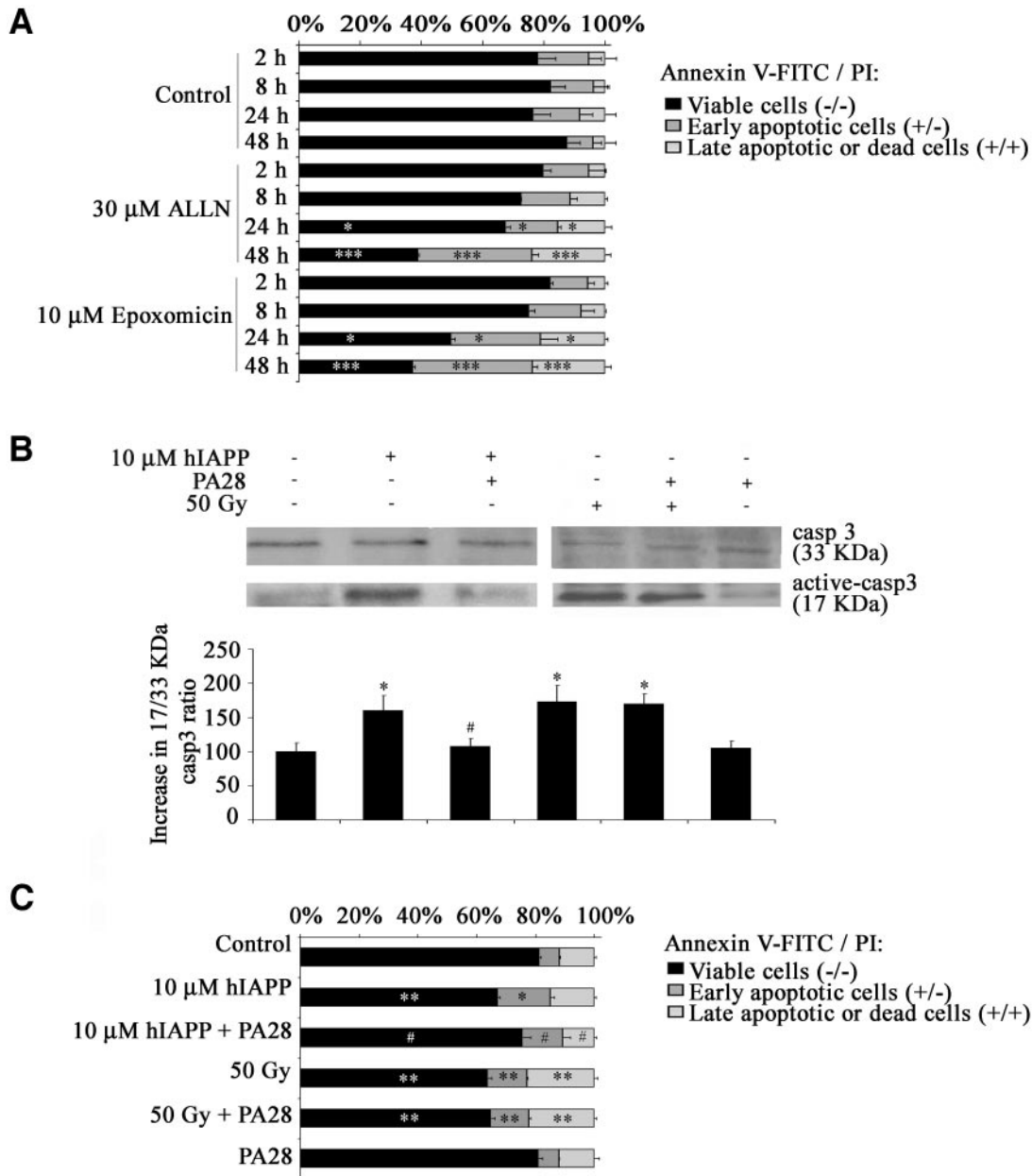


**FIG. 5.** Effect of proteasome activity on MIN6 cells. **A:** Apoptosis assay of MIN6 cells with proteasome-dependent proteolysis inhibition by 30  $\mu$ M ALLN or 10  $\mu$ M epoxomicin. Control MIN6 cells were cultured with vehicle solution. Cell staining with annexin V-FITC and PI was analyzed by FACS. Results are means  $\pm$  SD ( $n = 4$ ) (\* $P < 0.05$ , \*\* $P < 0.001$ ; by ANOVA). **B and C:** Apoptosis assay of MIN6 cells with proteasome-dependent proteolysis activation. MIN6 cells were transfected with 10  $\mu$ g PA28 or vehicle for 4 h before exposure to 10  $\mu$ M hIAPP for 16 h. Apoptosis-positive controls, namely 50 Gy irradiated MIN6 cells, were included in each experiment. **B:** Western blot specific for caspase 3 (casp3) and active casp3. Results of protein quantification are means  $\pm$  SD ( $n = 6$ ) (\* $P < 0.05$  vs. control, # $P < 0.05$  vs. 10  $\mu$ M hIAPP; by Mann-Whitney test). **C:** Cell staining with annexin V-FITC and PI was analyzed by FACS. Results are means  $\pm$  SD ( $n = 6$ ) (\* $P < 0.05$  vs. control, \*\* $P < 0.01$  vs. control, # $P < 0.05$  vs. 10  $\mu$ M hIAPP; by Mann-Whitney test).

sion of ER chaperones during ER stress responses (18). The spliced active form of *Xbp-1* has been detected at basal levels in islet  $\beta$ -cells and increased in response to ER stress, indicating that it may be important for maintenance of  $\beta$ -cell ER function (36). Increased expression of *sXbp-1* was found in MIN6 cells early after hIAPP treatments, suggesting a rapid activation of ER responses. Consistent with these findings, abnormal ultrastructural morphology of the ER was observed in treated MIN6 cells. These data suggested that extracellular hIAPP may cause protein misfolding and ER stress. Our results are in agreement with recent findings that have revealed intracellular signaling such as ER stress related to extracellular amyloid-

osis, attributed to the capacity of amyloid peptides to elevate intracellular calcium and alter the redox status (29–31).

A sustained elevation of intracellular calcium was observed in 39% of MIN6 cells during 2-h incubations with hIAPP, which was frequently followed by cell detachment. It is likely that formation of hIAPP aggregates was required for deregulation of intracellular calcium homeostasis, since the effect was observed before fibril formation and did not occur with rIAPP. In light of the alterations in plasma membrane morphology, it is possible that the interaction of hIAPP aggregates with the plasma membrane may be an essential



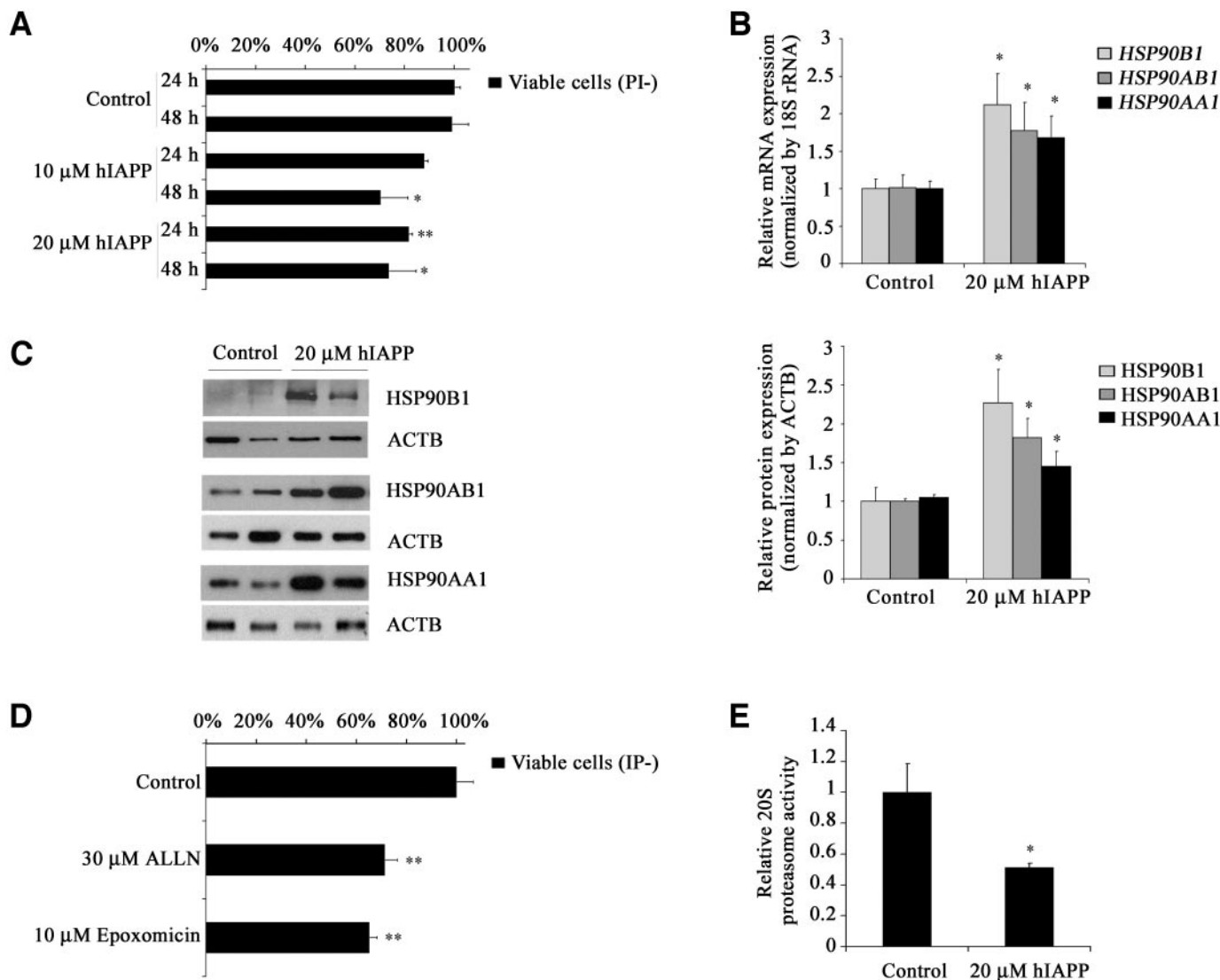


**FIG. 6.** Effect of extracellular hIAPP on human pancreatic islets. **A:** Human pancreatic islets were cultured with 10 or 20 μmol/l hIAPP for 24 and 48 h. Cell viability assays were performed on dispersed islet cells stained with PI and analyzed by FACS. Results are means ± SD ( $n = 4$ ) (\* $P < 0.05$ , \*\* $P < 0.01$ ; by Mann-Whitney test). **B:** Quantification of *HSP90AA1*, *HSP90AB1*, and *HSP90B1* mRNA expression in human pancreatic islets treated with 20 μmol/l hIAPP for 48 h compared with the control. Results are means ± SD ( $n = 6$ ) (\* $P < 0.05$  by Mann-Whitney test). **C:** Quantification of *HSP90AA1*, *HSP90AB1*, and *HSP90B1* protein expression in human pancreatic islets treated with 20 μmol/l hIAPP for 48 h compared with the control analyzed by immunoblot. Membranes were stripped and immunoblotted with anti-β-actin (ACTB) antibody. Representative images of  $n = 6$ . Results of protein level quantification are means ± SD ( $n = 6$ ) (\* $P < 0.05$  by Mann-Whitney test). **D:** Cell viability assay on human pancreatic islets treated with proteasome-dependent proteolysis inhibition by 30 μmol/l ALLN or 10 μmol/l epoxomicin compared with the vehicle control for 48 h. Dispersed islet cells stained with PI were analyzed by FACS. Results are means ± SD ( $n = 4$ ) (\*\* $P < 0.01$  by Mann-Whitney test). **E:** Protein extracts from intact human pancreatic islets cultured with 20 μmol/l hIAPP for 24 h and control were tested in a fluorometric 20S proteasome proteolytic activity assay. Results are means ± SD ( $n = 6$ ) (\* $P < 0.05$  by Mann-Whitney test).

step in this process. Although a previous study did not detect elevated calcium levels in insulinoma cells treated with hIAPP for 2–8 h (37), cells that were poorly adherent or detached following a calcium rise may have been excluded from their analysis due to washing steps before the measurement of calcium accumulation. Nevertheless, our results are supported by reports suggesting that amyloid peptides may initiate cytotoxicity in neurons by inducing alterations in the plasma membrane (15,16,24,26), which lead to elevated intracellular calcium levels (16,23,27,28,30).

It is possible that intracellular calcium overload induced by extracellular hIAPP preceded ER dysfunction in MIN6-cells. ER resident chaperones actually require adequate ER calcium concentrations for their activity; thus, changes in ER calcium homeostasis may trigger accumulation of

misfolded proteins and activation of ER stress responses (18). Moreover, most mitochondrial and cytosolic ROS-generating enzymes are regulated by calcium, and excessive intracellular calcium concentrations might enhance ROS production, which interferes with the correct synthesis and folding of proteins (18).

Efficient removal of misfolded proteins via the ubiquitin-proteasome pathway is essential for cellular recovery during ER stress responses. However, when ER stress defenses are unable to restore ER function, accumulation of unfolded proteins can collapse the proteasome, leading to decreased proteasome activities (19,38,39). By quantifying the proteasome function of MIN6 cells treated with hIAPP, we detected a significant reduction in the proteasomal proteolytic activity over time, which contributed to the intracellular accumulation of ubiquitinated proteins,

leading to a functional suppression of the ubiquitin-proteasome pathway. Reduced proteasome activity was also observed in primary cultures of human pancreatic islets treated with hIAPP. These data suggest that failure of the ubiquitin-proteasome pathway was an event downstream of the ER stress response induced by extracellular hIAPP oligomers. To date, dysregulation of the ubiquitin-proteasome pathway has been implicated in neurodegenerative diseases (40–44). Analyses of human brains in Alzheimer's disease have shown decreases in the proteasome activities in association with intracellular deposition of aggregated and ubiquitinated proteins (40,43). In addition, it is likely that dysregulation of the ubiquitin-proteasome pathway in neurons is mediated by extracellular deposition of  $\beta$ -amyloid plaques (45).

In the present study, we have demonstrated that impairment of the proteasome function by pharmacological treatment contributes to apoptosis in MIN6 cells. Reduced cell viability was also observed in primary cultures of human pancreatic islets treated with different proteasome inhibitors. In agreement with our results, apoptosis was previously reported in several  $\beta$ -cell lines under inhibition of proteasome function (46). However, the authors showed that proteasome inhibition had no impact on rat islet cell viability (46). This apparent discrepancy with our findings could probably be attributed to either the different nature or the concentration of the proteasome inhibitors used. In support of our data, previous studies of the involvement of the ubiquitin-proteasome system in vivo also showed substantial sensitivity of the pancreas to proteasome inhibition (47). Moreover, stimulation of proteasome activity by delivery of PA28 significantly reduced apoptosis and substantially decreased the activation of caspase-3 induced by extracellular hIAPP. Activation of caspase-3 is known to function in the programmed cell death pathway of hIAPP-mediated cytotoxicity (48). Taken together, the data suggest that the decline of the ubiquitin-proteasome pathway could be considered as an upstream activator of apoptotic signaling for pancreatic  $\beta$ -cells exposed to extracellular hIAPP. Induction of apoptosis by proteasome inactivation has also been observed in neurodegenerative models (49) and seems to be dependent on the loss of mitochondrial membrane potential (50).

In conclusion, our study indicates that ER stress responses are involved in the pancreatic  $\beta$ -cell apoptosis induced by extracellular hIAPP. The data demonstrate that dysregulation of the ubiquitin-proteasome pathway should be considered a potential link between the ER stress due to plasma membrane perturbation by extracellular hIAPP aggregate formation and the degeneration of pancreatic  $\beta$ -cells by apoptosis.

#### ACKNOWLEDGMENTS

This study was supported by Fondo de Investigación Sanitaria (FIS) (PI05/1327, PI05/1215), Red de Grupos en Diabetes Mellitus (RGDM) (G03/212), and Red de Diabetes y Enfermedades Metabólicas Asociadas (REDIMET) (RD06/0015) grants from the Ministerio de Sanidad y Consumo in Spain, the Academy of Finland, and the Sigrid Jusélius Foundation in Finland. S.C. is recipient of a Juan de la Cierva contract from the Ministerio de Educación y Ciencia in Spain and an Albert Renold Fellowship from the

European Foundation for the Study of Diabetes. F.M.G. is funded by the Wellcome Trust.

The authors thank Marta Julià for technical assistance.

#### REFERENCES

1. Westermark P, Grimelius L: The pancreatic islet cells in insular amyloidosis in human diabetic and non-diabetic adults. *Acta Pathol Microbiol Scand A* 81:291–300, 1973
2. Howard CF Jr: Longitudinal studies on the development of diabetes in individual *Macaca nigra*. *Diabetologia* 29:301–306, 1986
3. Westermark P, Wernstedt C, Wilander E, Hyden DW, O'Brien TD, Johnson KH: Amyloid fibrils in human insulinoma and islets of Langerhans of the diabetic cat are derived from a neuropeptide-like protein also present in normal islet cells. *Proc Natl Acad Sci U S A* 84:3881–3885, 1987
4. Clark A, Cooper GJ, Lewis CE, Morris JF, Willis AC, Reid KB, Turner RC: Islet amyloid formed from diabetes-associated peptide may be pathogenic in type-2 diabetes. *Lancet* 2:231–234, 1987
5. Kahn SE, D'Alessio DA, Schwartz MW, Fujimoto WY, Ensink JW, Tabor-sky GJ Jr, Porte D Jr: Evidence of cosecretion of islet amyloid polypeptide and insulin by beta-cells. *Diabetes* 39:634–638, 1990
6. Novials A, Sarri Y, Casamitjana R, Rivera F, Gomis R: Regulation of islet amyloid polypeptide in human pancreatic islets. *Diabetes* 42:1514–1519, 1993
7. Gasa R, Gomis R, Casamitjana R, Novials A: Signals related to glucose metabolism regulate islet amyloid polypeptide (IAPP) expression in human pancreatic islets. *Regul Pept* 68:99–104, 1997
8. Westermark P, Engström U, Johnson KH, Westermark GT, Betsholtz C: Islet amyloid polypeptide: pinpointing amino acid residues linked to amyloid fibril formation. *Proc Natl Acad Sci U S A* 87:5036–5040, 1990
9. Sakagashira S, Hiddinga HJ, Tateishi K, Sanke T, Hanabusa T, Nanjo K, Eberhardt NL: S20G mutant amylin exhibits increased in vitro amyloidogenicity and increased intracellular cytotoxicity compared to wild type amylin. *Am J Pathol* 157:2101–2109, 2000
10. Novials A, Rojas I, Casamitjana R, Usac EF, Gomis R: A novel mutation in islet amyloid polypeptide (IAPP) gene promoter is associated with type II diabetes mellitus. *Diabetologia* 44:1064–1065, 2001
11. Hull RL, Westermark GT, Westermark P, Kahn SE: Islet amyloid: a critical entity in the pathogenesis of type 2 diabetes. *J Clin Endocrinol Metab* 89:3629–3643, 2004
12. Lorenzo A, Razzaboni B, Weir GC, Yankner BA: Pancreatic islet cell toxicity of amylin associated with type-2 diabetes mellitus. *Nature* 368:756–760, 1994
13. Janson J, Soeller WC, Roche PC, Nelson RT, Torchia AJ, Kreutter DK, Butler PC: Spontaneous diabetes mellitus in transgenic mice expressing islet amyloid polypeptide. *Proc Natl Acad Sci U S A* 93:7283–7288, 1996
14. Butler AE, Jang J, Gurlo T, Carty MD, Soeller WC, Butler PC: Diabetes due to a progressive defect in  $\beta$ -cell mass in rats transgenic for human islet amyloid polypeptide (HIP rat): a new model for type 2 diabetes. *Diabetes* 53:1509–1516, 2004
15. Janson J, Ashley RH, Harrison D, McIntyre S, Butler PC: The mechanism of islet amyloid polypeptide toxicity is membrane disruption by intermediate-sized toxic amyloid particles. *Diabetes* 48:491–498, 1999
16. Demuro A, Mina E, Kaye R, Milton SC, Parker I, Glabe CG: Calcium dysregulation and membrane disruption as a ubiquitous neurotoxic mechanism of soluble amyloid oligomers. *J Biol Chem* 280:1794–17300, 2005
17. Meier JJ, Kaye R, Lin CY, Gurlo T, Haataja L, Jayasinghe S, Langen R, Glabe CG, Butler PC: Inhibition of human IAPP fibril formation does not prevent  $\beta$ -cell death: evidence for distinct actions of oligomers and fibrils of human IAPP. *Am J Physiol Endocrinol Metab* 291:E1317–E1324, 2006
18. Rao RV, Ellerby HN, Bredesen DE: Coupling endoplasmic reticulum stress to cell death program. *Cell Death Differ* 11:372–380, 2004
19. McClellan AJ, Tam S, Kaganovich D, Frydman J: Protein quality control: chaperones culling corrupt conformations. *Nat Cell Biol* 7:736–741, 2005
20. Glickman MH, Ciechanover A: The ubiquitin-proteasome pathway: destruction of the sake of construction. *Physiol Rev* 82:373–428, 2002
21. Ciechanover A: Proteolysis: from the lysosome to ubiquitin and the proteasome. *Nat Rev Mol Cell Biol* 6:79–87, 2005
22. Araki E, Oyadomari S, Mori M: Impact of endoplasmic reticulum stress pathway on pancreatic beta-cells and diabetes mellitus. *Exp Biol Med (Maywood)* 228:1213–1217, 2003
23. Mattson MP, Goodman Y: Different amyloidogenic peptides share a similar mechanism of neurotoxicity involving reactive oxygen species and calcium. *Brain Res* 676:219–224, 1995

24. Mirzabekov TA, Lin MC, Kagan BL: Pore formation by the cytotoxic islet amyloid peptide amylin. *J Biol Chem* 271:1988–1992, 1996
25. Porat Y, Kolusheva S, Jelinek R, Gazit E: The human islet polypeptide forms transient membrane-active prefibrillar assemblies. *Biochemistry* 42:10971–10977, 2003
26. Sparr E, Engel MF, Sakharov DV, Sprong M, Jacobs J, de Kruijff B, Hoppener JW, Killian JA: Islet amyloid polypeptide-induced membrane leakage involves uptake of lipids by forming amyloid fibers. *FEBS Lett* 577:117–120, 2004
27. Bucciantini M, Calloni C, Chiti F, Formigli L, Nosi D, Dobson CM, Stefani M: Prefibrillar amyloid protein aggregates share common features of cytotoxicity. *J Biol Chem* 279:31374–31382, 2004
28. Cecchi C, Baglioni S, Fiorillo C, Pensalfini A, Liguri G, Nosi D, Rigacci S, Bucciantini M, Stefani M: Insights into the molecular basis of the differing susceptibility of varying cell types to the toxicity of amyloid aggregates. *J Cell Sci* 118:3459–3470, 2005
29. Nakagawa T, Zhu H, Morishima N, Li E, Xu J, Yankner BA, Yuan J: Caspase-12 mediates endoplasmic-reticulum-specific apoptosis and cytotoxicity by amyloid-β. *Nature* 403:98–103, 2000
30. Pereira C, Ferreira E, Cardoso SM, de Oliveira CR: Cell degeneration induced by amyloid-beta peptides: implication for Alzheimer's disease. *J Mol Neurosci* 23:97–104, 2004
31. Teixeira PF, Cerca F, Santos SD, Saraiva MJ: Endoplasmic reticulum stress associated with extracellular aggregates: evidence from transthyretin deposition in familial amyloid polyneuropathy. *J Biol Chem* 281:21998–22003, 2006
32. Ishihara H, Asano T, Tsukuda K, Katagiri H, Inukai K, Anai M, Kikuchi M, Yazaki Y, Miyazaki JI, Oka Y: Pancreatic β-cell line MIN6 exhibits characteristics of glucose metabolism and glucose-stimulated insulin secretion similar to those of normal islets. *Diabetologia* 36:1139–1145, 1993
33. Coronado-Pons I, Novials A, Casas S, Clark A, Gomis R: Identification of iduronate-2-sulfatase in mouse pancreatic islets. *Am J Physiol Endocrinol Metab* 287:E983–E990, 2004
34. Dantuma NP, Lindsten K, Glas R, Jellne M, Masucci MG: Short-lived green fluorescent proteins for quantifying ubiquitin/proteasome-dependent proteolysis in living cells. *Nat Biotechnol* 18:538–543, 2000
35. Csermely P, Schnaider T, Soti C, Prohaszka Z, Nardai G: The 90-KDa molecular chaperone family: structure, function and clinical applications: a comprehensive review. *Pharmacol Ther* 79:129–168, 1998
36. Nozaki J, Kubota H, Yoshida H, Naitoh M, Goji J, Yoshinaga T, Mori K, Koizumi A, Nagata K: The endoplasmic reticulum stress response is stimulated through the continuous activation of transcription factors ATF6 and XBP1 in Ins2<sup>+Akita</sup> pancreatic β-cells. *Genes Cells* 9:261–270, 2004
37. Bai JZ, Saafi EL, Zhang S, Cooper GJS: Role of Ca<sup>2+</sup> in apoptosis evoked by human amylin in pancreatic islet β-cells. *Biochem J* 343:53–61, 1999
38. Keller JN, Hanni KB, Markesbery WR: Impaired proteasome function in Alzheimer's disease. *J Neurochem* 75:436–439, 2000
39. Bence NF, Sampat RM, Kopito RR: Impairment of the ubiquitin-proteasome system by protein aggregation. *Science* 292:1552–1555, 2001
40. Keller JN, Hanni KB, Markesbery WR: Possible involvement of proteasome inhibition in aging: implication for oxidative stress. *Mech Ageing Dev* 113:61–70, 2000
41. Lam YA, Pickart CM, Alban A, Landon M, Jamieson C, Ramage R, Mayer RJ, Layfield R: Inhibition of ubiquitin-proteasome system in Alzheimer's disease. *Proc Natl Acad Sci U S A* 97:9902–9906, 2000
42. McNaught KS, Jenner P: Proteasomal function is impaired in substantia nigra in Parkinson's disease. *Neurosci Lett* 297:191–194, 2001
43. Waelter S, Boeddrich A Lurz R, Scherzinger E, Lueder G, Lehrach H, Wanker EE: Accumulation of huntingtin fragments in aggresome-like inclusion bodies as a result of insufficient protein degradation. *Mol Biol Cell* 12:1393–1407, 2001
44. Ma J, Wollmann R, Lindquist S: Neurotoxicity and neurodegeneration when PrP accumulates in the cytosol. *Science* 298:1781–1785, 2002
45. Song S, Kim SY, Hong YM, Jo DG, Lee JY, Shim SM, Chung CW, Seo SJ, Yoo YJ, Koh JY, Lee MC, Yates AJ, Ichijo H, Jung YK: Essential role of E2-25K/Hip-2 in mediating amyloid-β neurotoxicity. *Mol Cell* 12:553–563, 2003
46. Størling J, Allaman-Pillet N, Karlens AE, Billestrup N, Bonny C, Mandrup-Poulsen T: Antitumorigenic effect of proteasome inhibitors on insulinoma cells. *Endocrinology* 146:1718–1726, 2005
47. Lindsten K, Menendez-Benito V, Masucci M, Dantuma NP: A transgenic mouse model of the ubiquitin/proteasome system. *Nat Biotechnol* 21:897–902, 2003
48. Rumora L, Hadzija M, Barisic K, Maysinger D, Grubiic TZ: Amylin-induced cytotoxicity is associated with activation of caspase-3 and MAP kinases. *Biol Chem* 383:1751–1758, 2002
49. Tanaka Y, Engelender S, Igarashi S, Rao RK, Wanner T, Tanzi RE, Sawa A, Dawson V, Dawson TM, Ross CA: Inducible expression of mutant alpha-synuclein decreases proteasome activity and increases sensitivity to mitochondria-dependent apoptosis. *Hum Mol Genet* 10:919–926, 2001
50. Valente EM, Abou-Sleiman PM, Caputo V, Muqit MM, Harvey K, Gispert S, Ali Z, Del Turco D, Bentivoglio AR, Healy DG, Albanese A, Nussbaum R, Gonzalez-Maldonado R, Deller T, Salvi S, Cortelli P, Gilks WP, Latchman DS, Harvey RJ, Dallapiccola B, Auburger G, Wood NW: Hereditary early-onset Parkinson's disease caused by mutations in *PINK1* gene. *Science* 304:1158–1160, 2004